Pharmaceutical Research (2024) 41:1233–1245
https://doi.org/10.1007/s11095-024-03709-y

ORIGINAL RESEARCH ARTICLE

Development of Amorphous Solid Dispersion Sustained-Release Formulations with Polymer Composite Matrix-Regulated Stable Release Plateaus

Lingwu Chen[1,2] · Enshi Hu[3] · Peiya Shen[3] · Shuai Qian[1] · Weili Heng[1] · Jianjun Zhang[3] · Yuan Gao[1] · Yuanfeng Wei[1]

Received: 15 February 2024 / Accepted: 21 April 2024 / Published online: 14 May 2024

Abstract

Purpose This study was designed to develop ibuprofen (IBU) sustained-release amorphous solid dispersion (ASD) using polymer composites matrix with drug release plateaus for stable release and to further reveal intrinsic links between polymer' matrix ratios and drug release behaviors.

Methods Hydrophilic polymers and hydrophobic polymers were combined to form different composite matrices in developing IBU ASD formulations by hot melt extrusion technique. The intrinsic links between the mixed polymer matrix ratio and drug dissolution behaviors was deeply clarified from the dissolution curves of hydrophilic polymers and swelling curves of composite matrices, and intermolecular forces among the components in ASDs.

Results IBU + ammonio methacrylate copolymer type B (RSPO) + poly(1-vinylpyrrolidone-co-vinyl acetate) (PVP VA64) physical mixtures presented unstable release behaviors with large error bars due to inhomogeneities at the micrometer level. However, IBU-RSPO-PVP VA64 ASDs showed a "dissolution plateau phenomenon", i.e., release behaviors of IBU in ASDs were unaffected by polymer ratios when PVP VA64 content was 35%~50%, which could reduce risks of variations in release behaviors due to fluctuations in prescriptions/processes. The release of IBU in ASDs was simultaneously regulated by the PVP VA64-mediated "dissolution" and RSPO-PVP VA64 assembly-mediated "swelling". Radial distribution function suggested that similar intermolecular forces between RSPO and PVP VA64 were key mechanisms for the "dissolution plateau phenomenon" in ASDs at 35%~50% of PVP VA64.

Conclusions This study provided ideas for developing ASD sustained-release formulations with stable release plateau modulated by polymer combinations, taking full advantages of simple process/prescription, ease of scale-up and favorable release behavior of ASD formulations.

Keywords amorphous solid dispersion · drug release plateau · hot melt extrusion technology · polymer composite matrix · sustained-release regulation

Lingwu Chen and Enshi Hu contributed equally in the experimental works.

✉ Jianjun Zhang
myamicute@163.com

✉ Yuan Gao
newgaoyuan@163.com

✉ Yuanfeng Wei
weiyuanfengyuer@yeah.net

[1] School of Traditional Chinese Pharmacy, China Pharmaceutical University, Nanjing 211198, People's Republic of China

[2] Jiuhua & Huayuan Pharmaceutical Co., Ltd, Chuzhou 239000, People's Republic of China

[3] School of Pharmacy, China Pharmaceutical University, Nanjing 211198, People's Republic of China

Introduction

At present, sustained-release formulations that can be industrially produced are mainly divided into matrix system [1, 2], membrane-controlled type [3], and osmotic pump type [4] sustained-release formulations according to the formulation process. However, the skeletal types have poor control over the release of water-soluble/insoluble drugs, showing abrupt release behavior [5, 6] and incomplete terminal release [7–9], respectively. For membrane control types, the screening of film material types (satisfying the sustained release requirement of API) and coating parameters is complex [10]. The osmotic pump formulation of insoluble drugs requires complex process design [11], such as the number of chambers and the number/pore size of orifices, to regulate

drug release rate [12]. It has been reported that the drug release is modulated by different ratios of hydrophilic and hydrophobic component combinations, usually showing a trend that the higher the ratio of hydrophilic component, the faster the release of the drug, but also faces the risk of unstable release due to local inhomogeneity [13, 14].

Amorphous solid dispersion (ASD), a homogeneous dispersion system where drugs in amorphous state highly dispersed in polymer carriers [15], is attracting growing interest in the development of sustained-release formulations due to its simple preparation process and prescription, ease of scale up, and solubility/dissolution advantages [16]. Currently, ASD sustained-release formulations usually use hydrophobic polymers as carriers, such as ethyl cellulose [17–19], ammonio methacrylate copolymer series [20, 21], and polylactic acid-hydroxy acetic acid copolymer [22, 23], but often face risks of extremely slow drug release rates or incomplete drug release at the endpoint because the forces (including hydrogen bonding [propranolol-eudragit L ASD [24]], electrostatic force [nitrendipine-HPMCP ASD [25]], and van der Waals forces [lopinavir-eudragit RL ASD [9]] between the insoluble polymers and the drug molecules are too large and inhibit the hydrogen bonding between the drug and water molecules [9, 26]. To address this issue, some hydrophilic polymers such as polyvinylpyrrolidone [8, 27] and polyethylene glycol [28] are often incorporated into hydrophobic polymer carriers to achieve modulation of drug release in ternary hydrophobic polymer-hydrophilic polymer-drug ASDs. Many reports [17, 20, 29, 30] have used this approach to modulate the release of ASDs, where the rate of drug release increases with the proportion of water-soluble polymers, implying that small variations in polymer ratios can significantly affect the dissolution behavior of drugs and thus lead to unstable qualities of ASD formulations. For example, Li and Lu *et al*. [29, 31]. demonstrated that a change of about 5% in the hydrophilic polymer content (20% → 25%) could affect drug release by 10–20% fluctuation. Literature study reveals a total of four reports [20, 21, 29, 30] on modulation of drug release from ASD formulations by mixing matrices. However, the reports mainly focused on formulation development, but there is a lack of research at the molecular level on the mechanisms of polymer-polymer blend matrices affecting drug release. Moreover, the intrinsic link between the ratio of polymer-polymer blend matrix and drug dissolution behavior has not been revealed. It is evident that there is a need to develop a highly durable ASD sustained-release formulation with a drug release plateau, to obtain a stable release behavior without being obviously affected by small changes in matrix ratios during production.

In this study, hydrophilic polymer poly(1-vinylpyrrolidone-co-vinyl acetate) (Fig. 1A, PVP VA64), hydrophilic polymer poly(ethylene glycol)-poly(vinyl acetate)-poly(vinyl caprolactam) graft copolymer (Soluplus), hydrophobic polymer ammonio methacrylate copolymer type B (Fig. 1B, RSPO), and hydrophobic polymer ethyl cellulose (EC) were combined to form different composite matrices (RSPO-Soluplus, EC-PVP VA64 and RSPO-PVP VA64) in the development of ibuprofen (Fig. 1C, IBU, BCS II drug) ASD formulations by hot melt extrusion (HME) technique, respectively. ASDs using the first two polymer composite matrices showed conventional release trends, i.e., the higher the proportion of water-soluble polymers, the faster the drug release, in agreement with literature reports [29]. Differently, the ASD based on RSPO-PVP VA64 composite matrix showed a "polymer ratio interval for stable drug release (drug release plateau phenomenon: variations in the amount of polymer within a certain range didn't change the IBU release behavior)", i.e., the drug release behavior in ASDs was approximately the same at a proportion 32.5%-50% of PVP VA64. However, RSPO + PVP VA64 + IBU physical mixtures did not show such drug release plateau phenomenon, but approximately linear release accompanied by large error bars. The intrinsic relationship between RSPO-PVP VA64 ratio and the dissolution behavior of IBU in ASDs was deeply clarified from the co-regulation of the dissolution of PVP VA64 with the swelling of RSPO-PVP VA64 and the differences in intermolecular forces between ASD systems. This study provided new ideas for developing ASD sustained-release formulations with stable release plateau modulated by polymer combinations.

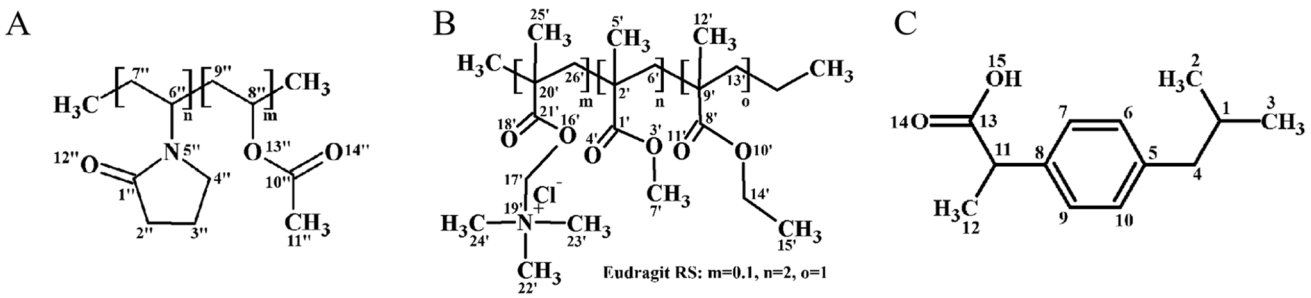

Fig. 1 Molecular structures of (**A**) poly(1-vinylpyrrolidone-co-vinyl acetate) (PVP VA64), (**B**) ammonio methacrylate copolymer type B (RSPO) and (**C**) ibuprofen (IBU).

Materials and Methods

Materials

IBU (purity > 99%) was acquired from Shandong Xinhua Pharmaceutical Co., Ltd (Jinan, China). PVP VA64 and Soluplus were purchased from BASF Pharm Co., Ltd. (Ludwigshafen, Germany). RSPO was received from Evonik Industries AG Co., Ltd. (Darmstadt, Germany). EC was received from Merck KGaA (Darmstadt, Germany). All other chemical reagents were purchased from Sinopharm Chemical Reagent Co., Ltd. (Shanghai, China).

HME Processing

IBU-RSPO-PVP VA64 ASDs, IBU-RSPO-Soluplus ASDs and IBU-EC-PVP VA64 ASDs with various mass ratios were prepared using a co-rotating twin-screw extruder (PPS TSE Elf, Pharmaceutical Processing Solution Co., Ltd, China) with a functional length of 20:1 L/D and a die opening of 3 mm diameter. The used screw configuration consists of the conveying element and mixing element with an offset angle of 60°. Before extrusion, all mixtures (IBU:RSPO:PVP VA64 = 3:0.5:6.5, 3:1:6, 3:1.5:5.5, 3:1.75:5.25, 3:2:5, 3:2.5:4.5, 3:3:4, 3:3.5:3.5, 3:3.75:3.25, 3:4:3, 3:5:2, and 3:6:1, w/w/w, equivalent to 65%, 60%, 55%, 52.5%, 50%, 45%, 40%, 35%, 32.5%, 30%, 20% and 10% PVP VA64; IBU:RSPO:Soluplus = 3:1:6, 3:2:5, 3:3:4 and 3:4:3, equivalent to 60%, 50%, 40% and 30% Soluplus; IBU:EC:PVP VA64 = 3:1:6, 3:2:5, 3:3:4 and 3:4:3, equivalent to 60%, 50%, 40% and 30% PVP VA64) were blended for 10 min using a three-dimensional mixer (SBH-1, Xinbao Co. Ltd., China). Subsequently, the obtained uniform mixtures were added into the hopper at the feeding rate of 1.0 g/min and screw speed of 20 rpm. The barrel temperature in zone I (i.e., the feeding zone) was set at 30°C, and the temperatures in zones II-IV with the same setting were 120°C. After cooling at room temperature, the extrudates were ground with mortar and passed through a sieve of 60 mesh for further analysis. In addition, RSPO-PVP VA64 extrudates (1:6, 2:5, 3:4 and 4:3, w/w) were prepared and post-treated under the same conditions as described above for subsequent studies. In addition, IBU + RSPO + PVP VA64 physical mixtures (1:6, 2:5, 3:4 and 4:3, w/w, equivalent to 60%, 50%, 40% and 30% PVP VA64) were prepared by blending for 10 min using a three-dimensional mixer (SBH-1, Xinbao Co. Ltd., China).

Differential Scanning Calorimetry (DSC)

Thermal analysis of samples was carried out using DSC 250 (TA Instruments, USA). The high purity indium standard was used to calibrate the temperature and heat flow. Nitrogen gas at a flow rate of 50 mL/min was used as the purge gas. About 3 mg of samples [IBU-RSPO-PVP VA64 extrudates, IBU-RSPO-Soluplus extrudates and IBU-EC-PVP VA64 extrudates] crimped in hermetic aluminum DSC pans were heated at a heating rate of 10°C/min in the range of 20–200°C. The data obtained were analyzed using TRIOS (version 5.1.1).

Fourier Transform-Raman Mapping (FT-Raman Mapping)

The Raman imaging allows spectra acquisition on a micro scale according to Raman shift of component to be monitored and provides selective information of component distribution and uniformity. The characteristic Raman peak of *p*-disubstituted benzene ring in IBU at 829.36 cm^{-1} was chosen to analyze the distribution homogeneity of IBU molecules in IBU-RSPO-PVP VA64 ASD and IBU + RSPO + PVP VA64 physical mixture. FT-Raman mapping tests were carried out with Horiba Raman spectroscopy microscopes (LabRAM HR Evolution, Horiba, Japan), spatial resolution was 0.65 cm^{-1}. The area maps were taken at 45 μm × 45 μm with 5 μm microns step (total 100 points). The Raman spectra of samples were collected by using 532 nm excitation light source with single exposure time of 1 s at room temperature. Spectral maps were analyzed using Lab Spec 6 software.

Dissolution Test

Dissolution tests were performed in triplicate by a dissolution apparatus (RC806D, Tianda Tianfa, China) using a paddle method. About 0.167 g of IBU-RSPO-PVP VA64 ASD, IBU-RSPO-Soluplus ASD and IBU-EC-PVP VA64 ASD powders (equivalent to 50 mg IBU), and 0.167 g of IBU + RSPO + PVP VA64 physical mixture powders (equivalent to 50 mg IBU) were added to 900 mL pure water (Millipore Corporation, USA) at 37°C, respectively. The rotating speed was set at 100 rpm. Five millilitre aliquots were withdrawn at predetermined time points (0.08, 0.17, 0.25, 0.33, 0.5, 0.75, 1, 1.5, 2, 3, 4, 6, 8, 12, 16 and 24 h), and then the same volume of fresh media was replenished. After filtered through 0.45 μm nylon filter (Millipore, Bedford, MA), the drug content of aliquots was measured using a UV-vis spectrophotometer (TU-1901, PERSEE, China) after appropriate dilution. The obtained time-dissolution data of samples were further fitted with Korsmeyer-Peppas equation (Eq. 1) [32]:

$$\frac{C_t}{C_\infty} = Kt^n \quad (1)$$

where C_t and C_∞ are the absolute cumulative amount of drug released at time t and infinite time, respectively; K is a constant incorporating structural and geometric characteristics of the preparation, and n is the release exponent, indicative of the drug release mechanism.

In addition, another set of dissolution experiments for IBU-RSPO-PVP VA64 ASDs were carried out under above conditions, where solid residues in the dissolution cups were collected at 0.17 h, 2 h, and 5 h and vacuum-dried for 24 h at room temperature to remove moisture for further SEM characterization.

Scanning Electron Microscopy (SEM)

The morphologies of IBU-RSPO-PVP VA64 ASDs after dissolution were observed by SEM (Phenom Pure$^+$, Thermo Fisher Scientific Inc., USA). The samples were fixed on metal sample plates using carbon double sided tape, and then sprayed gold (thickness: 15–20 nm) by a SC502 sputter coater (Fission Instruments, UK) for 10 min at 2.0 kV electrical potential and 25 mA current, to enhance electrons reflection of samples surface. SEM measurements were performed at 10.0 kV with 4000-folds and 9000-folds magnification.

Swelling Curve of RSPO-PVP VA64 Composite Matrix and Dissolution Curve of PVP VA64

About 250 mg RSPO-PVP VA64 extrudate powders (1:6, 2:5, 3:4 and 4:3, w/w) were further pressed into tablets ($\Phi \approx 13$ mm, $\delta \approx 5$ mm) by hydraulic press at pressure of 74 Mpa. The tablets were placed in 30 mL of pure water at 37 ± 0.5°C, using a water bath thermostatic shaker (SHZ-B, Guowang Instrument Manufacturing Co., LTD, China) at a stirring speed of 100 rpm. At each sampling point (0.5 h, 1 h, 2 h, 3 h, 4 h, 6 h, 8 h, and 12 h), the tablets were collected, and vacuum filtrated to remove surface moisture. The tablet was weight as M_w, and then vacuum dried to a constant weight (M_d) (the process is detailed in Fig. S1) [29].

The swelling rate was characterized by equilibrium water content ($EW\%$) and calculated as Eq. 2:

$$EW\% = \frac{M_W - M_\mathrm{d}}{M_\mathrm{d}} \times 100\% \tag{2}$$

The degree of PVP VA64 erosion rate ($ER\%$) was determined based on the mass difference between initial point and the experimental time point t (Eq. 3):

$$ER\% = \frac{M_i - M_\mathrm{d}}{M_\mathrm{i} \times k} \times 100\% \tag{3}$$

where M_i represents the initial weight of tablets and k represents the theoretical mass fraction of VA64.

Radial Distribution Function (RDF) Calculations

Molecular dynamics (MD) simulation was used to further analyze intermolecular interaction sites and possibilities among components of ASDs. RDF via MD simulation is an effective analytical method to probe the structure information of materials by calculating the local spatial distribution and giving the probability density g(r) of the occurrence of other atoms at a certain distance from the reference atom [33–35]. All MD simulations were performed under NPT and NVT ensembles with a time step of 1 fs and a period of 400 ps [36] using the Amorphous cell and Forcite module of Material Studio 9.0 software in COMPASS II. The van der Waals were calculated using Atom Based and Ewald methods.

The simulation procedure details were shown as follows: (1) The amorphous cells were constructed which containing IBU, RSPO, and PVP VA64 molecules respectively; (2) The constructed amorphous cells continued to be geometrically optimized and then went through dynamics simulations under NPT and NVT ensembles with a set of temperature at 120°C by the Andersen method, for analyzing the interactions between components of ASDs during extrusion; (3) The quench simulation was carried out under NVT ensemble at 25°C, for the objective of calculating interactions between components of ASDs during cooling at room temperature; (4) For investigating the effect of medium on the interactions among components of ASDs during dissolution, water molecules were introduced into the simulation process. In detail, a layer model including the amorphous cells of ASDs as the first layer and the amorphous cell of 2000 water molecules as the second layer were constructed, and the NVT ensemble was used to run the layer model dynamically with a set temperature of 37°C (i.e., the medium temperature). After finishing above MD simulations, RDF analysis was performed by calculating g(r) values between the electron donor and electron acceptor groups of component molecules by using the Analysis function in the Forcite module. The schematic diagram of RDF analysis using MD simulation was shown in Fig. S2.

Results

DSC

The DSC curves of IBU-RSPO-PVP VA64 extrudates with various mass ratios were shown in Fig. 2. Only one single T_g was observed at 87.32–90.07°C in each system, suggesting the successful preparation of IBU-RSPO-PVP VA64 (65%, 60%, 55%, 52.5%, 50%, 45%, 40%, 35%, 32.5%, 30%, 20% and 10% PVP VA64) ASDs. It could be found that the T_g values of the ASDs were not significantly changed by the ratio of RSPO-PVP VA64. T_g as an

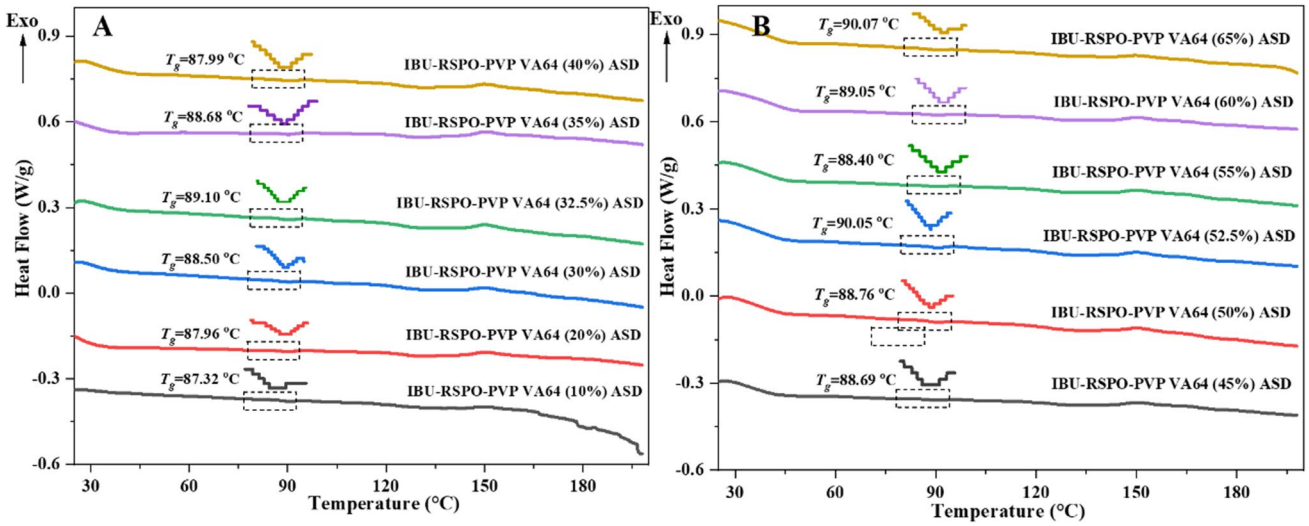

Fig. 2 DSC curves of IBU-RSPO-PVP VA64 ASDs with various mass ratios (**A**: 10%~40% PVP VA64, **B**: 45%~65% PVP VA64).

inherent property of amorphous materials, which is the lowest temperature at which the molecular chain segments can move. Its value is directly related to the flexibility of the molecular chain, the greater the molecular chain flexibility, the lower the value of T_g; the greater the molecular chain rigidity, the higher the value of T_g [37]. The PVP VA64 molecule is a co-polymerization of vinyl pyrrolidone monomer and vinyl acetate monomer, and RSPO is a co-polymerization of methacrylate monomer and quaternary amine monomers (Fig. 1), showing that their molecular chains do not contain rigid structures, and therefore, the ratio of RSPO-PVP VA64 did not have obvious effects on the T_g values of the ASDs. In addition, the specific single T_g data of IBU-RSPO-Soluplus ASDs and IBU-EC-PVP VA64 ASDs were shown in Table S1.

FT-Raman Mapping

IBU-RSPO-PVP VA64 ASD showed a distinctive characteristic peak at 829.36 cm^{-1} (Fig. S3), which was attributed to the *p*-disubstituted benzene ring in IBU [38, 39]. Therefore, the FT-Raman mapping of the *p*-disubstituted benzene in IBU was measured at 829.36 cm^{-1} to investigate the distribution of IBU molecules in IBU-RSPO-PVP VA64 ASD and IBU + RSPO + PVP VA64 physical mixture. As shown in Fig. 3, the red area meant strong scattering intensity from high concentration of the *p*-disubstituted benzene in IBU and the purple area revealed the low concentration of the *p*-disubstituted benzene ring in IBU, suggesting that IBU molecules were uniformly distributed in the ASD system but obviously aggregated in the physical mixture.

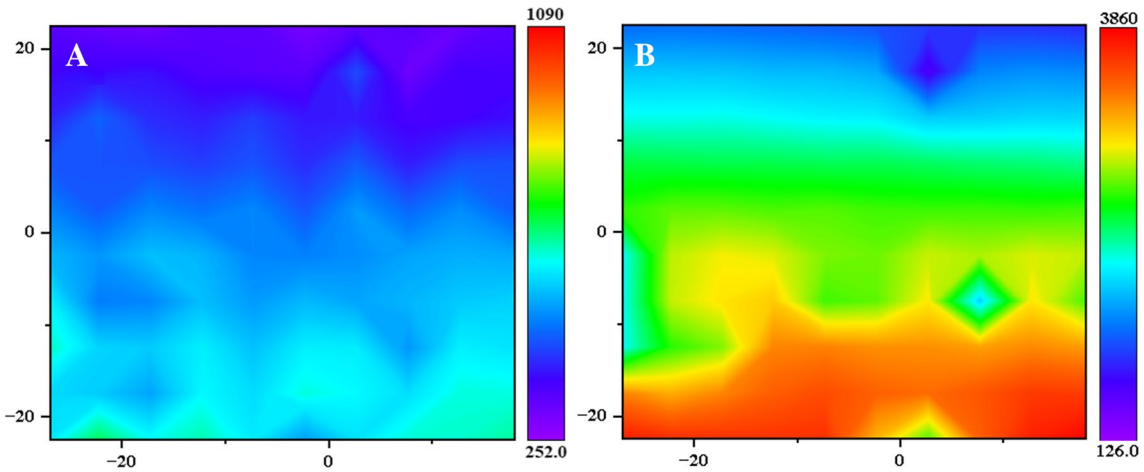

Fig. 3 The FT-Raman mapping of the *p*-disubstituted benzene ring in IBU from (**A**) IBU-RSPO-PVP VA64 ASD and (**B**) IBU + RSPO + PVP VA64 physical mixture.

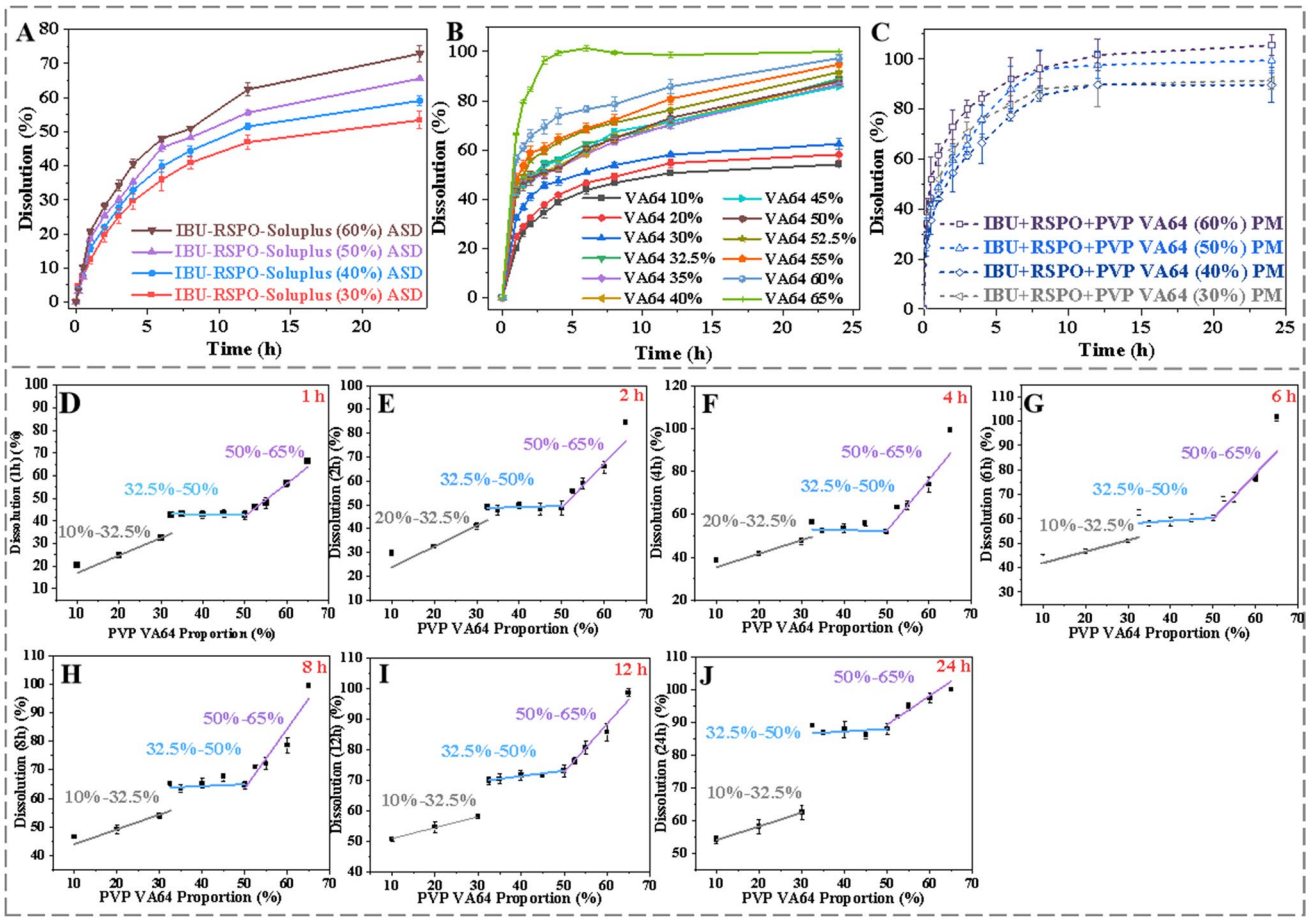

Fig. 4 (**A**) Dissolution curves of IBU from IBU-RSPO-Soluplus ASDs in water at 37°C. (**B**) Dissolution curves of IBU from IBU-RSPO-PVP VA64 ASDs in water at 37°C. (**C**) Dissolution curves of IBU from IBU + RSPO + PVP VA64 physical mixtures in water at 37°C. The curves of PVP VA64 mass ratio *versus* IBU dissolution at (**D**) 1 h, (**E**) 2 h, (**F**) 4 h, (**G**) 6 h, (**H**) 8 h, (**I**) 12 h, and (**J**) 24 h.

Dissolution Test

The dissolution profiles of IBU-RSPO-Soluplus ASDs were shown in Fig. 4A and dissolution profiles of IBU-EC-PVP VA64 ASDs were shown in Fig. S4. The dissolution of IBU from IBU-RSPO-Soluplus ASDs (30%, 40%, 50% and 60% Soluplus) and IBU-EC-PVP VA64 ASDs (30%, 40%, 50% and 60% PVP VA64) varied from 47% ~ 62%, 70% ~ 100% within 12 h, respectively. This indicated an obvious linear correlation between the polymer combination ratio and IBU dissolution, and a 5% variation in polymer ratio could induce changes in drug release behavior, consistent with literature reports [29, 31].

The dissolution profiles of IBU-RSPO-PVP VA64 ASDs were shown in Fig. 4B. The dissolution of IBU from IBU-RSPO-PVP VA64 ASDs (20% ~ 32.5%, 50% ~ 65% PVP VA64) was also routinely linear with the water-soluble polymer-PVP VA64 ratio. However, the dissolution behavior of IBU from IBU-RSPO-PVP VA64 ASDs (32.5% ~ 50% PVP VA64) was similar, with dissolution of IBU in these ASDs reaching ~ 43% in 1 h, ~ 70% in 12 h and ~ 88% at the end point of dissolution (24 h).

The curves for PVP VA64 mass ratio were fitted at low (20%-32.5%), middle (32.5%-50%) and high (50%-65%) segments to IBU dissolution at different time points (1, 2, 4, 6, 8, 12, and 24 h), respectively (Fig. 4D-J). Interestingly, the relationship between IBU dissolution and PVP VA64 ratio over 0–24 h at different time points all represented as a three-stage function. In detail, at high PVP VA64 ratio range (50%-65%) or low PVP VA64 ratio range (20%-32.5%), IBU dissolution at each time point was linearly related to the PVP VA64 ratio and enhanced by the growing hydrophilic polymers ratio. However, in the ASDs with medium PVP VA64 ratio range (32.5%-50%), IBU dissolution remained consistent at all time points even as the proportion of hydrophilic polymer increased. It could be seen that the above three-stage function break the traditional understanding that the higher the percentage of hydrophilic polymers, the faster the drug release, and the existence of this release plateau would improve the durability of ASD sustained-release formulations to obtain a stable release behavior. In addition, the relationship between IBU dissolution and PVP VA64 ratio over 0–24 h at different time

points all represented as a three-stage function in the dissolution medium at pH 1.2 and 6.8 (Fig. S5), which further proving that the type of polymer played a leading role.

The dissolution profiles of IBU + RSPO + PVP VA64 physical mixtures were shown in Fig. 4C. They could release completely within 8 h without good slow-release performance, and their dissolution behavior exhibited large SD values (Table S2), revealing that simple mixing did not enable polymer composites to modulate drug release and tended to cause large release variations due to local inhomogeneities.

SEM

The SEM profiles and phenomena diagrams of IBU-RSPO-PVP VA64 ASDs during dissolution was shown in Fig. 5 and Fig. S6, respectively, it was obvious that ASD containing more insoluble polymers exhibited more obvious swelling behavior macroscopically. TEM observations showed that the ASD systems, except for IBU-RSPO-PVP VA64 (60% PVP VA64) ASD, were porous and the pores became denser as the dissolution proceeded. In addition, more dense porous structures also were observed inside the system (9000×). However, the porosity effect was still different among the ASDs with different RSPO-PVP VA64 mass ratios. Specifically, the surface pore numbers of IBU-RSPO-PVP VA64 (30% PVP VA64) ASD during dissolution at 10 min and the internal pore numbers during dissolution at 5 h (~ 10058 pores) were higher than the other ASDs, accompanied with lower pore area to some extent. The porosity effect of IBU-RSPO-PVP VA64 (40% and 50% PVP VA64) ASDs was similar with large sparse pores appearing on their surfaces at 10 min of dissolution. As the dissolution proceeded, the surface pore numbers and area of the two ASDs became larger (40% PVP VA64: ~ 1557 *vs*. 50% PVP VA64: ~ 1469), and the pores gradually expanded to the interior. However, IBU-RSPO-PVP VA64 (60% PVP VA64) ASD seemed completely different from other ASDs in that its skeleton gradually collapsed during dissolution without pores forming. After 10 min of dissolution, the surface VA64 of

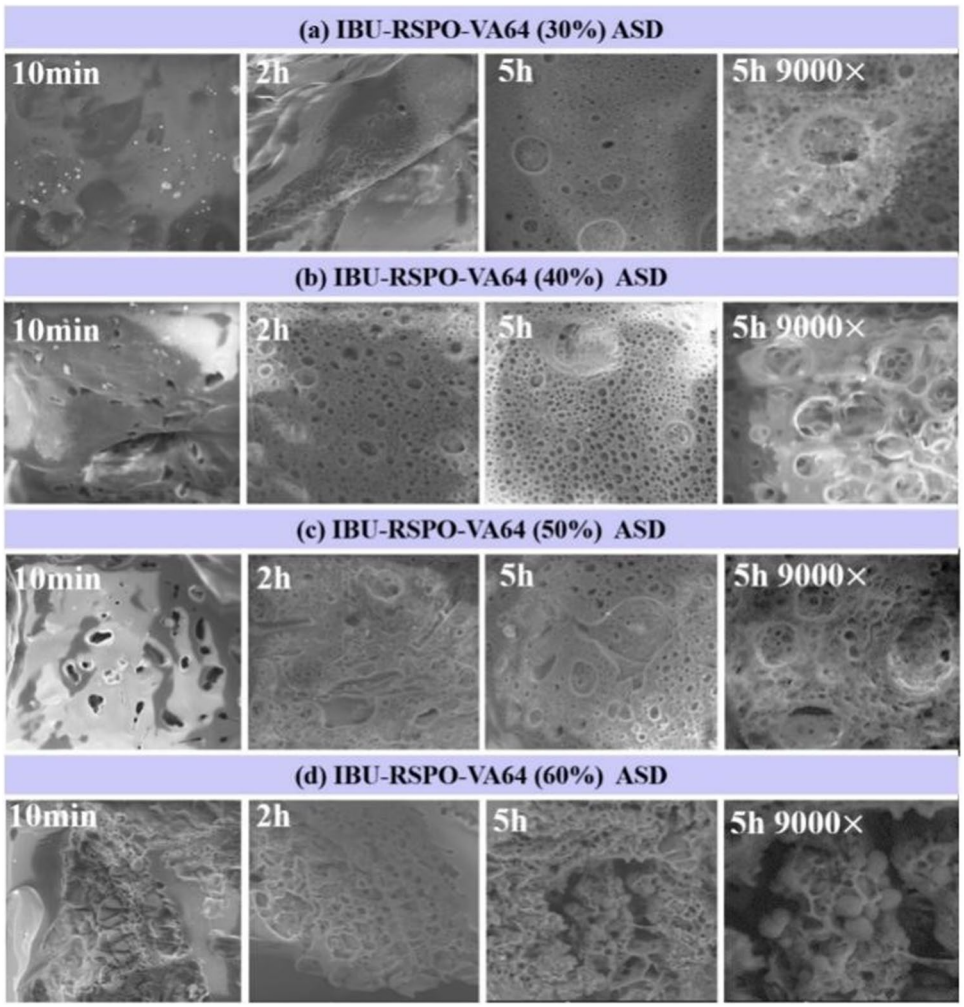

Fig. 5 Microstructures of IBU-RSPO-PVP VA64 [(**a**) 30%, (**b**) 40%, (**c**) 50% and (**d**) 60% PVP VA64] ASDs after 10 min (4000×), 2 h (4000×) and 5 h (4000× and 9000×) of dissolution.

IBU-RSPO-PVP VA64 (60% PVP VA64) ASD has been almost completely dissolved, showing a loose and sunken appearance with hardly observable intact pores.

Swelling Curve of RSPO-PVP VA64 Composite Matrix and Dissolution Curve of PVP VA64

The PVP VA64 dissolution curves of RSPO-PVP VA64 extrudates were shown in Fig. 6A. The PVP VA64 in RSPO-PVP VA64 (1:6) extrudate could almost completely dissolved at 4 h; and the dissolution behavior of PVP VA64 in RSPO-PVP VA64 (2:5 and 3:4) extrudates were similar, i.e., up to ~ 88% within 4 h, followed by slow dissolution until a plateau was reached after 12 h (~ 95%); The dissolution behavior of VA64 in RSPO-PVP VA64 (4:3) extrudate dissolved ~ 77% in 4 h and then gradually dissolved up to 90% at 12 h. It could be obtained that the PVP VA64 dissolution rate of RSPO-PVP VA64 extrudates was ordered as 1:6 > 2:5 ≈ 3:4 > 4:3.

The equilibrium water content curves of RSPO-PVP VA64 extrudates were shown in Fig. 6B. The dissolution of soluble polymers is a finite swelling → infinite swelling → dissolution process [40], meaning that the undissolved PVP VA64 in RSPO-PVP VA64 extrudates would absorb water and underwent finite swelling. It could be seen that the equilibrium water of RSPO-PVP VA64 extrudates was originated from RSPO and undissolved PVP VA64. The RSPO-PVP VA64 (1:6, 2:5 and 3:4) extrudates reached swelling equilibrium at 3, 6, and 8 h, respectively (~ 240%, ~ 130% and ~ 110%), while the equilibrium water content of RSPO-PVP VA64 (4:3) extrudate increased extremely slowly until the end point (~ 59%). It could be concluded that the equilibrium water content of RSPO-PVP VA64 extrudates was ranked as 1:6 > 2:5 ≈ 3:4 > 4:3, which was consistent with the ordering of the dissolution rate of PVP VA64 from RSPO-PVP VA64 extrudates.

RDF Calculations

The RDF calculations for IBU-RSPO-PVP VA64 ASDs were shown in Fig. 7 and Table S4-S5. RDF is an analytical method to analyze material structures by calculating the local spatial distribution, giving the probability density g(r) of the occurrence of other atoms at a certain distance from the reference atom, which provides a certain basis for studying intermolecular forces. If the distance between atoms is lower than 3.10 Å, the strong intermolecular interactions such as hydrogen bond are usually considered to form, and if the distance between atoms is 3.0–6.0, it is considered that there may be van der Waals force [41]. The number of interaction sites between RSPO and PVP VA64 in the ASDs was ranked as 20% = 30% > 35% = 40% = 50% > 55% > 60% (PVP VA64 ratio). Detailly, the same interaction sites were found in IBU-RSPO-PVP VA64 (20% and 30%) ASDs including RSPO-$N_{19'}$-PVP VA64-$N_{5''}$ [g(4.5) = 32 *vs* g(4.5) = 25], RSPO-$N_{19'}$-PVP VA64-$O_{14''}$ [g(4.4) = 30 *vs* g(4.4) = 24], RSPO-$N_{19'}$-PVP VA64-$O_{12''}$ [g(4.9) = 22 *vs* g(4.8) = 18] and RSPO-$N_{19'}$-PVP VA64-$O_{13''}$ [g(4.8) = 8 *vs* g(4.8) = 10]. IBU-RSPO-PVP VA64 (35%, 40% and 50%) ASDs presented same interaction sites and similar possibilities (RSPO-$N_{19'}$-PVP VA64-$N_{5''}$ [g(r) = 29–35], RSPO-$N_{19'}$-PVP VA64-$O_{12''}$ [g(r) = 24–28] and RSPO-$N_{19'}$-PVP VA64-$O_{12''}$ [g(r) = 14–16]). IBU-RSPO-PVP VA64 (55% and 60%) ASD systems contained fewer interaction sites compared to other ASDs (IBU-RSPO-PVP VA64 (55%) ASD: RSPO-$N_{19'}$-PVP VA64-$O_{14''}$ [g(4.4) = 24]; IBU-RSPO-PVP VA64 (60%)

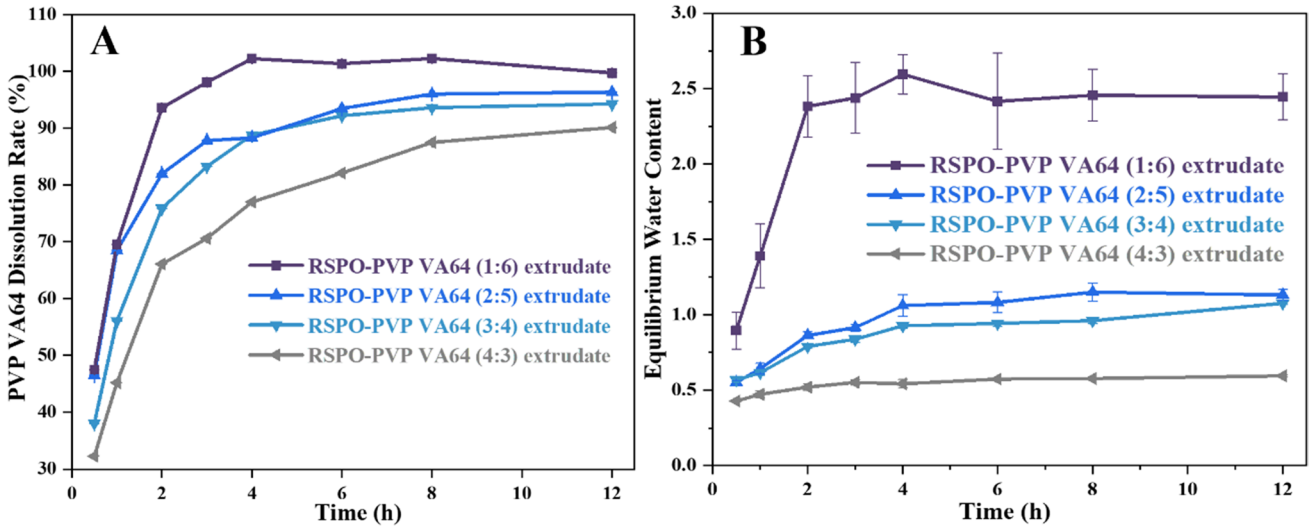

Fig. 6 (**A**) The PVP VA64 dissolution curves and (**B**) the equilibrium water content curves of RSPO-PVP VA64 extrudates.

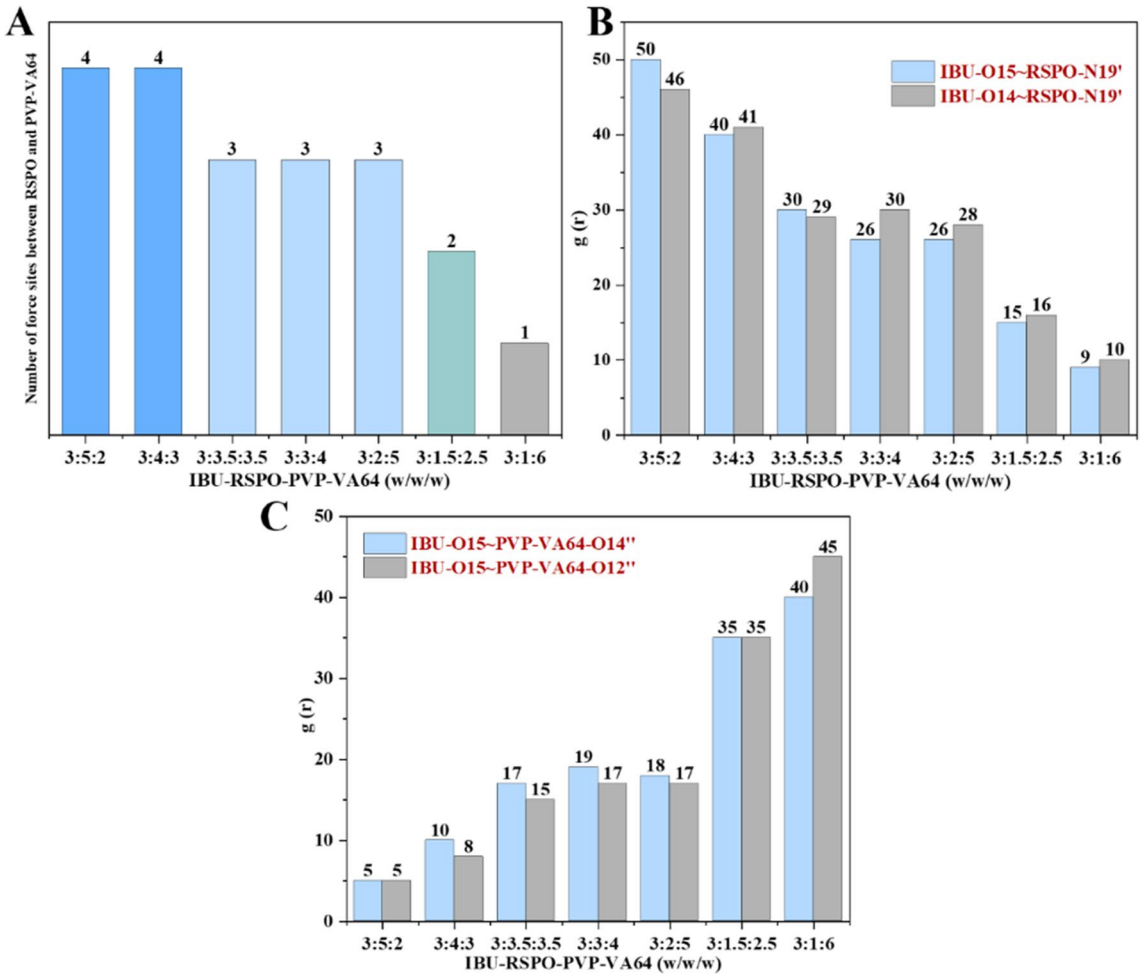

Fig. 7 (**A**) The number of force sites between RSPO and PVP VA64 in ASDs, the g(r) values of force sites (**B**) between IBU and RSPO and (**C**) IBU and PVP VA64 in ASDs.

ASD: RSPO-$N_{19'}$-PVP VA64-$N_{5''}$ [g(4.5) = 35]). The interaction sites between IBU and RSPO/PVP VA64 in the ASDs are the same, in which the interaction probabilities between IBU and RSPO (IBU-O_{15} ~ RSPO-$N_{19'}$, IBU-O_{14} ~ RSPO-$N_{19'}$) were ranked as 20% > 30% > 35% ≈ 40% ≈ 50% > 55% > 60%, while the interaction probabilities between IBU and PVP VA64 (IBU-O_{15}-PVP VA64-$O_{14''}$, IBU-O_{15}-PVP VA64-$O_{12''}$) were on the contrary, i.e. 20% < 30% < 35% ≈ 40% ≈ 50% < 55% < 60%. In presence of solvent system (water), compared to those of ASDs in absence of water, the interaction site among components of ASDs remained same, but the interaction possibilities were increased (RSPO-PVP VA64: g(r) = 30–61 *vs* g(r) = 8–35; IBU-RSPO: g(r) = 29–74 *vs* g(r) = 9–50; IBU-PVP VA64: g(r) = 34–73 *vs* g(r) = 5–45). It could be seen that van der Waals forces (r > 3.1) were generated among components in IBU-RSPO-PVP VA64 ASDs in absence of water and their possibilities were obviously enhanced in presence of water.

Discussion

The Release Plateau of IBU in IBU-RSPO-PVP VA64 ASDs at 35%-50% of PVP VA64

As shown in Fig. 4B, IBU-RSPO-PVP VA64 ASDs exhibited good sustained- release behavior within 24 h, agreeing with the Korsmeyer-Peppas drug release model (Fig. S7 and Table S6), and their dissolution behavior was linked with the ratio of polymer composites (Fig. 4D-J). The release exponent (*n*) was used to analyze dissolution behavior of drug preparations. It was generally considered that when $n < 0.43$, the drug release was dominated by Fickian diffusion mechanism; and when $0.43 < n < 0.85$, the drug release was more likely anomalous transport; and when $n > 0.85$, the drug was transported in case II [32]. The release exponent of IBU-RSPO-PVP VA64 ASDs was all between 0.10 and 0.26 (PVP VA64 mass ratio, 65%: 0.10, 60%: 0.16, 55%: 0.20, 52.5%: 0.21, 50%: 0.25,

45%: 0.22, 40%: 0.23, 35%: 0.13, 32.5%: 0.23, 30%: 0.19, 20%: 0.25, 10%: 0.26), revealing that the sustained-release behavior of IBU from ASDs were caused by the Fickian diffusion mechanism [42]. As clearly seen from the SEM images (Fig. 5), the ASDs during dissolution had differences in "pore" density. To further quantify the "pore density", since ImageJ software could not effectively distinguish the color of pores from the background in the TEM images, we manually counted the pores in TEM images of ASD products dissolved for 5 h, except for the ASD with 60% PVP VA64 that collapsed due to rapid dissolution. The results indicate that the order of pore area was 50% ≈ 40% > 30%, showing that the RSPO-PVP VA64 ratio played a dominant role in the pore effect. Further, the internal "pores" could be observed from images of ASDs (at 5 h of dissolution) magnified 9000 times. Hydrophilic PVP VA64 on the surface of ASD powders dissolved first, which facilitated the contact between RSPO and medium, causing the swelling of RSPO and undissolved PVP VA64 and the appearance of pores on the powder surface. As the dissolution proceeded, the medium entered the interior of powders through the pores, and the dissolution of internal PVP VA64 occurred, which further promoted the swelling phenomenon of the internal RSPO together with PVP VA64, resulting in the observation of pores in powder cores. In summary, the dissolution of PVP VA64 and swelling of RSPO-PVP VA64 matrix occurred simultaneously with dissolution, affecting drug release.

To further analyze how PVP VA64 and RSPO affect drug release, the swelling behavior of RSPO-PVP VA64 composite matrix and the dissolution behavior of PVP VA64 were quantitatively measured (Fig. 6). The dissolution rate of PVP VA64 and the swelling rate of RSPO-PVP VA64 in RSPO-PVP VA64 (1:6) extrudate system was much higher than that of the other systems, reaching a plateau at 2 h and remaining until the end point (12 h), once again proving the mutual influence between the dissolution behavior of PVP VA64 and the swelling behavior of RSPO-PVP VA64. The rapid dissolution of PVP VA64 made the contact between the system and medium more rapid and sufficient, promoting the swelling of the ASD system and facilitating the rapid release of IBU from the ASD. In RSPO-PVP VA64 (2:5 and 3:4) extrudate systems, the dissolution rate of PVP VA64 and swelling rate of RSPO-PVP VA64 were nearly identical, respectively, reaching a plateau at about 4 h and remaining until the end point, with a similar effect on the drug release and thus a similar IBU release profile. For the RSPO-PVP VA64 (4:3) extrudate system, both the dissolution rate of PVP VA64 and swelling rate of RSPO-PVP VA64 were much smaller than that of other systems, which obviously reduced the contact area between drugs and medium, resulting in low drug dissolution.

In summary, it can be concluded that the trend of the dissolution rate of PVP VA64 and the swelling rate curve of RSPO-PVP VA64 of each system remained consistent, which jointly affected the release of IBU; moreover, the order of the dissolution rate of PVP VA64 and the swelling rate of RSPO-PVP VA64 among the systems was consistent with the ordering of IBU release rate, indicating that they co-regulated the drug release.

The Necessity of System Molecular Mixing Homogeneity for Stable Release Behavior

As clearly seen from Fig. 4C, the dissolution of IBU from IBU + RSPO + PVP VA64 physical mixtures did not present considerable sustained-release behavior and showed an approximately linear relationship with the proportion of the polymer composite. However, it exhibited large SD values at each time point, implying that simple mixing was difficult to control drug dissolution by modulating the ratio of polymer composites. According to the results of Raman mapping (Fig. 3), the *p*-disubstituted phenyl group of IBU molecules in the ASD system was uniformly distributed without differences in intensity, meaning the uniform distribution of IBU molecules in the ASD at the molecular level. In contrast, in the IBU + RSPO + PVP VA64 physical mixtures, there were obvious differences in the intensity of the *p*-disubstituted phenyl of IBU molecules, implying the non-uniform distribution of IBU molecules in the physical mixtures. It could be assumed that in the ASD system, the IBU molecules and polymer molecules could achieve homogeneity of mixing at the molecular level, facilitating the mixed matrix to jointly coordinate the release of IBU from ASD formulations. However, the IBU particles occurred as micron-scale aggregated state in physical mixture, and thus could not make sufficient contact with the surrounding polymers, which made it difficult for the polymer mixture to fully regulate the release of IBU molecules. Therefore, the uniform distribution of ASDs at molecular level was conducive to the drug diffusion regulating by polymer composites.

On the other hand, the RDF calculations for ASDs and physical mixtures were performed to further investigate the interactions between components (Fig. 7, Table S3 and S4). The interaction sites between IBU and RSPO/PVP VA64 were the same in ASDs [IBU-O_{15} ~ RSPO-$N_{19'}$, IBU-O_{14} ~ RSPO-$N_{19'}$, IBU-O_{15}-PVP VA64-$O_{14''}$ and IBU-O_{15}-PVP VA64-$O_{12''}$]. The number of interaction sites between RSPO and PVP VA64 varied with the polymer ratio in the order of 20% = 30% > 35% = 40% = 50% > 55% > 60% (PVP VA64 ratio). It is evident that there are sufficient interactions among three components in ASDs, which provided full possibilities for the polymer composite to influence the release of IBU molecules. Further, the correlation between the number of interaction sites between RSPO and PVP VA64 and the ratio of RSPO-PVP VA64 implied the potential for co-coordination of IBU release by mixed polymers. However, the interactions among components in physical mixtures were not correlated with the

ratio of RSPO-PVP VA64 (Table S3). In IBU + RSPO + PVP VA64 (60% and 50%) physical mixtures, van der Waals forces were observed between IBU and PVP VA64 (IBU- O_{15}-PVP VA64-$O_{14''}$, IBU- O_{15}-PVP VA64-$O_{12''}$), while no interaction was observed between IBU and RSPO. In IBU + RSPO + PVP VA64 (40% and 30%) physical mixtures, van der Waals forces were found between IBU and RSPO (IBU-O_{15}-PVP VA64-$O_{14''}$, IBU-O_{15}-PVP VA64-$O_{12''}$), but no interaction was generated between IBU and PVP VA64. Meanwhile, the number of interaction sites between RSPO and PVP VA64 showed obvious irregularities with their ratios, where the order was ranked as 40% (RSPO-$N_{19'}$-PVP VA64-$N_{5''}$, RSPO-$N_{19'}$-PVP VA64-$O_{14''}$, RSPO-$N_{19'}$-PVP VA64-$O_{12''}$ and RSPO-$N_{19'}$-PVP VA64-$O_{13''}$, g(r) = 6 ~ 12) > 30% (RSPO-$N_{19'}$-PVP VA64-$N_{5''}$, RSPO-$N_{19'}$-PVP VA64-$O_{14''}$ and RSPO-$N_{19'}$-PVP VA64-$O_{12''}$, g(r) = 9 ~ 11) > 50% (RSPO-$N_{19'}$-PVP VA64-$N_{5''}$ and RSPO-$N_{19'}$-PVP VA64-$O_{14''}$, g(r) = 12 ~ 13) > 60% (RSPO-$N_{19'}$-PVP VA64-$N_{5''}$, g(r) = 7). It could be obtained that there were no sufficient interactions between the components in IBU + RSPO + PVP VA64 physical mixtures as ASDs, which was mainly due to the inhomogeneous mixing of the components at the molecular level.

In summary, it was clear that the homogeneous mixing of the components in ASDs at the molecular level facilitated adequate intermolecular interactions among RSPO, PVP VA64 and IBU (Fig. 8), providing the possibility that the combined RSPO-PVP VA64 matrix could stably modulate the release of IBU from ASDs. However, the inhomogeneity of IBU + RSPO + PVP VA64 physical mixtures at the micrometer level affected the sufficient intermolecular interactions between the components, which led to large dissolution errors bar.

The Influence Mechanism of Polymer Combination Ratio on the Regulation of Drug Release

The intrinsic mechanism of RSPO-PVP VA64 composite co-coordinated IBU release was analyzed from the perspective of intermolecular interactions by RDF calculations (Table S4 and S5). The interaction sites between IBU and RSPO/PVP VA64 during dissolution (IBU-O_{15} ~ RSPO-$N_{19'}$, IBU-O_{14} ~ RSPO-$N_{19'}$, IBU-O_{15}-PVP VA64-$O_{14''}$ and IBU-O_{15}-PVP VA64-$O_{12''}$) were the same as those before dissolution, and the interaction possibilities increased [g(r) = 5–50 *vs* g(r) = 29–74]. It could be seen that the presence of aqueous medium promoted intermolecular contact between the components, allowing the swelling of RSPO-PVP VA64 and the dissolution of PVP VA64 to further affect the release of IBU. Meanwhile, the van der Waals force strength between RSPO and PVP VA64 in the ASDs was enhanced during dissolution compared to that before dissolution [g(r) = 8–35 *vs* g(r) = 30–61], and the interaction sites remained unchanged (Table S4 and S5). The increase in van der Waals force strength between RSPO (RSPO-$N_{19'}$) and PVP VA64 (PVP VA64-$N_{5''}$, PVP VA64-$O_{12''}$, PVP VA64-$O_{13''}$ and PVP VA64-$O_{14''}$) would impede the contact between PVP VA64 molecules and water molecules, decreasing the dissolution rate of PVP VA64, as well as decreasing the swelling rate of the system by hindering the diffusion of water molecules into the interior of the ASDs. The IBU-RSPO-PVP VA64 (50%, 40% and 35% PVP VA64) ASDs with similar dissolution behavior of IBU had the same interaction sites (RSPO-$N_{19'}$-PVP VA64-$N_{5''}$, RSPO-$N_{19'}$-PVP VA64-$O_{14''}$ and RSPO-$N_{19'}$-PVP VA64-$O_{12''}$) and similar interaction possibilities [g(r) = 31–61 *vs* g(r) = 34–57 *vs* g(r) = 35–58], revealing that the similar intermolecular interactions between RSPO and PVP VA64 components in ASDs promote stable release behavior, and are the key mechanism of the "stable release plateau phenomenon", which has been further validated by indomethacin-RSPO-PVP VA64 ASD system (Fig. S8) and rotundine- RSPO-PVP VA64 ASD system (Fig. S9). Furthermore, it is noteworthy that the interaction of RSPO with PVP VA64 in IBU-RSPO-PVP VA64 (60%, 55%, 30% and 20% PVP VA64) ASDs was obviously linked with their ratios, i.e., the higher the mass ratio of RSPO, the higher the number/

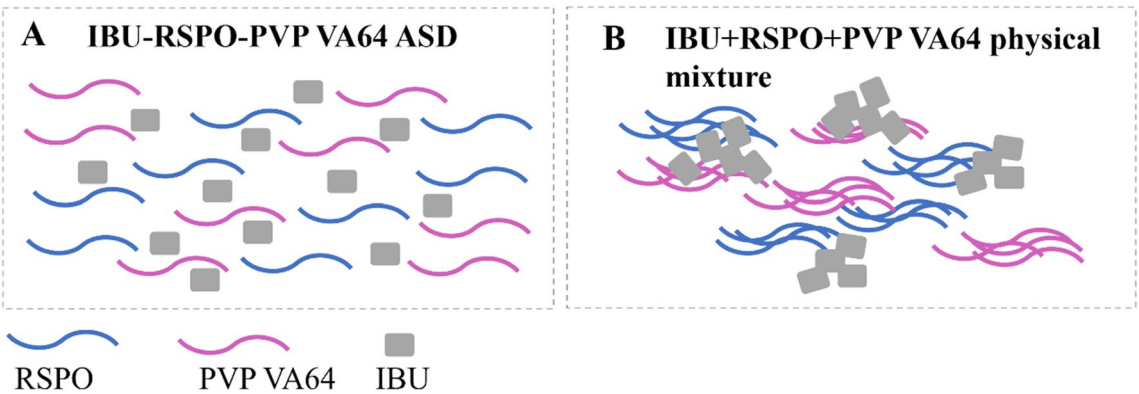

Fig. 8 Distribution diagram of component molecules (**A**) in ASDs and (**B**) physical mixtures.

probability of inter-polymer interaction, implying that as the mass ratio of RSPO increased, the intermolecular interactions between RSPO and PVP VA64 were enhanced thus inhibiting the dissolution of PVP VA64 and reducing the release of IBU. In summary, it could be concluded that the macroscopic dissolution-swelling behavior of the polymer composite and the microscopic intermolecular forces between components in ASDs during dissolution were closely linked with the polymer composite ratio, which together coordinated the release behavior of IBU from the ASDs.

Conclusion

It has been reported in the literature as well as found in this study that small variations in component ratios may cause ASD sustained-release formulations based on polymer combination matrices to exhibit obvious fluctuations in release behavior, implying that variations in prescription may trigger unstable drug release in industrial production. In this study, IBU + RSPO + PVP VA64 physical mixtures presented unstable release behaviors with large error bars due to inhomogeneities at the micrometer level. However, IBU-RSPO-PVP VA64 ASDs showed a "dissolution plateau phenomenon", i.e., the release behavior of IBU in ASDs was unaffected by the polymer ratio when the PVP VA64 content was 35% ~ 50%, which could reduce the risk of variations in the release behavior due to fluctuations in the prescription/process. It was found that the release of IBU in ASDs was simultaneously regulated by the PVP VA64-mediated "dissolution" and RSPO-PVP VA64 assembly-mediated "swelling". RDF calculations further suggested that similar intermolecular forces between RSPO and PVP VA64 were the key mechanism for the "dissolution plateau phenomenon" in ASDs at 35% ~ 50% of PVP VA64, which has been validated with other drugs, providing new ideas for developing ASD sustained-release formulations with stable release plateau modulated by polymer combination.

Supplementary Information The online version contains supplementary material available at https://doi.org/10.1007/s11095-024-03709-y.

Author Contribution Lingwu Chen: Conceptualization, Data curation, Writing—Original Draft. Enshi Hu: Methodology, Data curation, Writing—Original draft. Peiya Shen: Methodology, Formal analysis, Investigation. Shuai Qian: Investigation, Visualization, Validation. Weili Heng: Project administration, Funding acquisition. Jianjun Zhang: Validation, Funding acquisition. Yuan Gao: Supervision, Writing—Review & Editing. Yuanfeng Wei: Supervision, Writing—Review & Editing, Funding acquisition.

Funding This work was supported by the National Natural Science Foundation of China (82373824, 82104401, 82274217, 82204636), the Natural Science Foundation of Jiangsu Province (SBK2020042291), "Double First-Class" University Project (3342100010, 2632021ZD15).

Data Availability Data will be made available on request.

Declarations

Competing Interest The authors declare no competing financial interest.

References

1. Nokhodchi A, Raja S, Patel P, Asare-Addo K. The role of oral controlled release matrix tablets in drug delivery systems. BioImpacts. 2012;2:175–87. https://doi.org/10.5681/bi.2012.027.
2. Prajapati SK, Jain A, Jain A, Jain S. Biodegradable polymers and constructs: a novel approach in drug delivery. Eur Polym J. 2019;120: 109191. https://doi.org/10.1016/j.eurpolymj.2019.08.018.
3. Hu LD, Liu Y, Tang X, Zhang Q. Preparation and in vitro/in vivo evaluation of sustained-release metformin hydrochloride pellets. Eur J Pharm Biopharm. 2006;64:185–192. https://doi.org/10.1016/j.ijpharm.2011.12.053.
4. Qin C, He W, Zhu CL, Wu MM, Jin Z, Zhang Q, Wang GJ, Yin LF. Controlled release of metformin hydrochloride and repaglinide from sandwiched osmotic pump tablet. Int J Pharm. 2014;466:276–85. https://doi.org/10.1016/j.ijpharm.2014.03.002.
5. Bibi A, Sadiqur R, Akhtar T, Akhtar K, Farooq M, Shahzad MI. Alginate-chitosan/MWCNTs nanocomposite: a novel approach for sustained release of Ibuprofen. J Poly Res. 2021;28:363. https://doi.org/10.1007/s10965-020-02342-8.
6. Bode C, Kranz H, Fivez A, Siepmann F, Siepmann J. Often neglected: PLGA/PLA swelling orchestrates drug release: HME implants. J Control Release. 2019;306:97–107. https://doi.org/10.1016/j.jconrel.2019.05.039.
7. Schver G, Nadvorny D, Lee PI. Evolution of supersaturation from amorphous solid dispersions in water-insoluble polymer carriers: Effects of swelling capacity and interplay between partition and diffusion. Int J Pharm. 2020;581: 119292. https://doi.org/10.1016/j.ijpharm.2020.119292.
8. Sun DD, Lee PI. Probing the mechanisms of drug release from amorphous solid dispersions in medium-soluble and medium-insoluble carriers. J Control Release. 2015;211:85-93. https://doi.org/10.1016/j.jconrel.2015.06.004.
9. Li N, Taylor LS. Tailoring supersaturation from amorphous solid dispersions. J Control Release. 2018;279:114–25. https://doi.org/10.1016/j.jconrel.2018.04.014.
10. Piao ZZ, Lee KH, Kim DJ, Lee HG, Lee J, Oh KT, Lee BJ. Comparison of release-controlling efficiency of polymeric coating materials using matrix-type casted films and diffusion-controlled coated tablet. AAPS PharmSciTech. 2010;11:630–6. https://doi.org/10.1208/s12249-010-9377-0.
11. Verma RK, Krishna DM, Garg S. Formulation aspects in the development of osmotically controlled oral drug delivery systems. J Control Release. 2002;79:7–27. https://doi.org/10.1016/S0168-3659(01)00550-8.
12. Li NN, Fan N, Wu B, Dai GL, Jiang CJ, Guo Y, Wang DL. Preparation and in vitro/in vivo evaluation of azilsartan osmotic pump tablets based on the preformulation investigation. Drug Dev Ind Pharm. 2019;45:1079–88. https://doi.org/10.1080/03639045.2019.1593441.
13. Liu CC, Li JB, Li K, Xie CF, Liu JD. Oxidized konjac glucomannan-cassava starch and sucrose esters as novel excipients for sustained-release matrix tablets. Int J Biol Macromol. 2010;156:1045–52. https://doi.org/10.1016/j.ijbiomac.2019.11.146.
14. Corti G, Cirri M, Maestrelli F, Mennini N, Mura P. Sustained-release matrix tablets of metformin hydrochloride in combination with triacetyl-β-cyclodextrin. Eur J Pharm Biopharm. 2008;68:303–9. https://doi.org/10.1016/j.ejpb.2007.06.004.

15. Duong TV, Van den Mooter G. The role of the carrier in the formulation of pharmaceutical solid dispersions part II: amorphous carriers. Expert Opin Drug Deliv. 2016;13:1681–94. https://doi.org/10.1080/17425247.2016.1198768.
16. Maincent J, Williams RO. Sustained-release amorphous solid dispersions. Drug Deliv Transl Res. 2018;8:1714–25. https://doi.org/10.1007/s13346-018-0494-8.
17. Yang Y, Wang H, Li H, Ou Z, Yang G. 3D printed tablets with internal scaffold structure using ethyl cellulose to achieve sustained ibuprofen release. Eur J Pharm Sci. 2018;115:11–8. https://doi.org/10.1016/j.ejps.2018.01.005.
18. Shi K, Salvage JP, Maniruzzaman M, Nokhodchi A. Role of release modifiers to modulate drug release from fused deposition modelling (FDM) 3D printed tablets. Int J Pharm. 2021;597: 120315. https://doi.org/10.1016/j.ijpharm.2021.120315.
19. Shin TH, Ho MJ, Kim SR, Im SH, Kim CH, Lee S, Kang MJ, Choi YW. Formulation and in vivo pharmacokinetic evaluation of ethyl cellulose-coated sustained release multiple-unit system of tacrolimus. Int J Biol Macromol. 2018;109:544–50. https://doi.org/10.1016/j.ijbiomac.2017.12.111.
20. Albarahmieh E, Qi S, Craig DQM. Hot melt extruded transdermal films based on amorphous solid dispersions in Eudragit RS PO: the inclusion of hydrophilic additives to develop moisture-activated release systems. Int J Pharm. 2016;514:270–81. https://doi.org/10.1016/j.ijpharm.2016.06.137.
21. Lee YS, Song JG, Lee SH, Han HK. Sustained-release solid dispersion of pelubiprofen using the blended mixture of aminoclay and pH independent polymers: preparation and in vitro/in vivo characterization. Drug Deliv. 2017;24:1731–9. https://doi.org/10.1080/10717544.2017.1399304.
22. Yoo HS, Oh JE, Lee KH, Park TG. Biodegradable nanoparticles containing doxorubicin-PLGA conjugate for sustained release. Pharm Res. 1999;16:1114–8. https://doi.org/10.1023/A:1018908421434.
23. Nieto K, Mallery SR, Schwendeman SP. Microencapsulation of amorphous solid dispersions of fenretinide enhances drug solubility and release from PLGA in vitro and in vivo. Int J Pharm. 2010;586: 119475. https://doi.org/10.1016/j.ijpharm.2020.119475.
24. Maniruzzaman M, Morgan DJ, Mendham AP, Pang JY, Snowden MJ, Douroumis D. Drug-polymer intermolecular interactions in hot-melt extruded solid dispersions. Int J Pharm. 2013;443(1–2):199–208. https://doi.org/10.1111/jphp.12183.
25. Wang LA, Cui FD, Hayase T, Sunada H. Preparation and evaluation of solid dispersion for nitrendipine-carbopol and nitrendipine-HPMCP systems using a twin screw extruder. Chem Pharm Bull. 2005;53(10):1240–5. https://doi.org/10.1248/cpb.53.1240.
26. Schver G, Nadvorny D, Lee PI. Evolution of supersaturation from amorphous solid dispersions in water-insoluble polymer carriers: Effects of swelling capacity and interplay between partition and diffusion. Int J Pharm. 2020;581: 119292. https://doi.org/10.1016/j.ijpharm.2020.119292.
27. Marks JA, Wegiel LA, Taylor LS, Edgar KJ. Pairwise polymer blends for oral drug delivery. J Pharm Sci. 2014;103:2871–83. https://doi.org/10.1002/jps.23991.
28. Nguyen TNG, Tran PHL, Vo TV, Duan W, Tran TTG. Development of a sustained release solid dispersion using swellable polymer by melting method. Pharm Res. 2016;33:102–9. https://doi.org/10.1007/s11095-015-1767-2.
29. Li Y, Lu M, Wu C. PVP VA64 as a novel release-modifier for sustained-release mini-matrices prepared via hot melt extrusion. Drug Deliv Transl Res. 2018;8:1670–8. https://doi.org/10.1007/s13346-017-0437-9.
30. Shergill M, Patel M, Khan S, Bashir A, McConville C. Development and characterisation of sustained release solid dispersion oral tablets containing the poorly water soluble drug disulfiram. Int J Pharm. 2016;497:3–11. https://doi.org/10.1016/j.ijpharm.2015.11.029.
31. Shi K, Salvage JP, Maniruzzaman M, Nokhodchi A. Role of release modifiers to modulate drug release from fused deposition modelling (FDM) 3D printed tablets. Int J Pharm. 2021;597: 120315. https://doi.org/10.1016/j.ijpharm.2021.120315.
32. Siepmann J, Peppas NA. Modeling of drug release from delivery systems based on hydroxypropyl methylcellulose (HPMC). Adv Drug Deliver Rev. 2001;48:139–57. https://doi.org/10.1016/j.addr.2012.09.028.
33. Wilmer CE, Kim KC, Snurr RQ. An extended charge equilibration method. J Phys Chem Lett. 2012;3:2506–11. https://doi.org/10.1021/jz3008485.
34. Panda DK, Bhargava BL. Molecular dynamics investigation of non-ionic deep eutectic solvents. J Mol Graph Model. 2022;113: 108152. https://doi.org/10.1016/j.jmgm.2022.108152.
35. Yang Y, Tang W, Liu S, Han D, Liu Y, Gong JJ. Solubility of benzoin in three binary solvent mixtures and investigation of intermolecular interactions by molecular dynamic simulation. J Mol Liq. 2017;243:472–83. https://doi.org/10.1016/j.molliq.2017.07.125.
36. Ren T, Chen J, Qi P, Xiao P, Wang P. Goserelin/PLGA solid dispersion used to prepare long-acting microspheres with reduced initial release and reduced fluctuation of drug serum concentration in vivo. Int J Pharm. 2022;615: 121474. https://doi.org/10.1016/j.ijpharm.2022.121474.
37. Kunal K, Robertson CG, Pawlus S, Hahn SF, Sokolov AP. Role of chemical structure in fragility of polymers: a qualitative picture. Macromolecules. 2008;41(19):7232–8. https://doi.org/10.1021/ma801155c.
38. Gera T, Smausz T, Kopniczky J, Galbács G, Ambrus R, Szabó-Révész P, Hopp B. Production of ibuprofen in crystalline and amorphous forms by Pulsed Laser Deposition (PLD). Appl Surf Sci. 2019;493:359–67. https://doi.org/10.1016/j.apsusc.2019.06.254.
39. Shi NQ, Lai HW, Zhang Y, Feng B, Xiao X, Zhang HM, Li ZQ, Qi XR. On the inherent properties of Soluplus and its application in ibuprofen solid dispersions generated by microwave-quench cooling technology. Pharm Dev Technol. 2018;23:573–86. https://doi.org/10.1080/10837450.2016.1256409.
40. Devotta I, Premnath V, Badiger MV, Rajamohanan PR, Ganapathy S, Mashelkar RA. On the dynamics of mobilization in swelling-dissolving polymeric systems. Macromolecules. 1994;27:532–9. https://doi.org/10.1021/ma00080a030.
41. Han P, Nie W, Zhao G, Gao P. Theoretical investigation on the structure and physicochemical properties of choline chloride-based deep eutectic solvents. J Mol Liq. 2022;366: 120243. https://doi.org/10.1016/j.molliq.2022.120243.
42. Pandey H, Parashar V, Parashar R, Prakash R, Ramteke PW, Pandey AC. Controlled drug release characteristics and enhanced antibacterial effect of graphene nanosheets containing gentamicin sulfate. Nanoscale. 2011;3:4104–8. https://doi.org/10.1039/C1NR10661A.